Dual metamaterial structures generated from an one-step fabrication using stencil lithography

Eunice S. P. Leong · J. Deng ·
Y. J. Liu · J. H. Teng

Abstract The flexibility to deposit metallic structures on any substrates without the need of lift-off or etching process are the main reasons for the recent popularity of using stencil lithography for plasmonic applications. In this work, we fabricate nanoholes on a Si_3N_4 membrane and deposit metal–dielectric layers and such approach allows us to have a perforated fishnet metamaterial structure on the membrane as well as its complementary pillar structure on a quartz substrate. We then studied and compared their optical properties from both experiment and simulation results.

1 Introduction

Metamaterials are artificially engineered structures that give rise to special optical properties. In the optical regime, most structures are made up of metal–dielectric layers with nanoscale features and the usual fabrication methods are e-beam lithography combined with lift-off and etching processes [1–5]. However, in the etching process, it may not be straightforward to have a system that can etch two different types of material efficiently; while in the lift-off process, for efficient liftoff to be carried out, the resist thickness should be at least half the thickness of the films to be deposited. It means high aspect ratio resist is required. To avoid these issues,
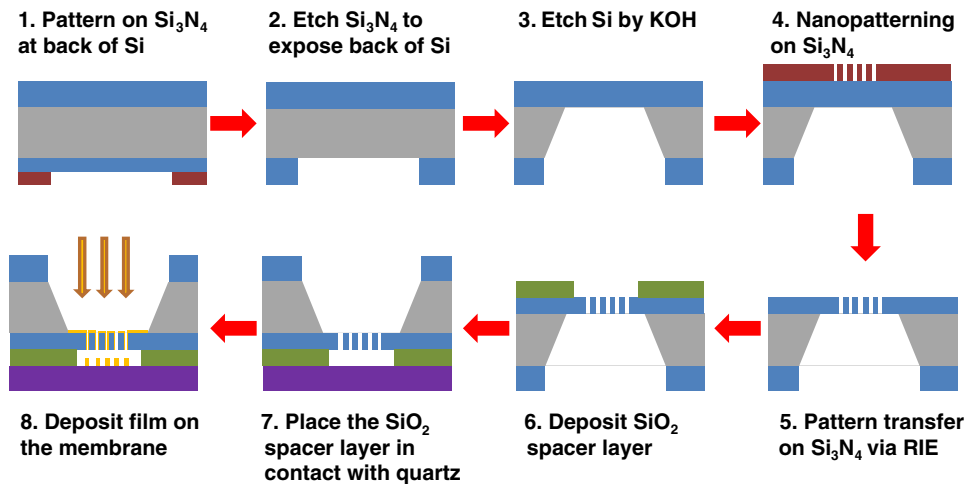
considerable advances in resistless nanopatterning have been reported recently based on transferring predefined nanostructures to diverse substrates using single- or multiple-step fabrication processes. High-quality micro/nanostructures have been demonstrated with high order and density using assembly [6–9], imprinting [10–13], and focused ion beam milling [14–17]. Beyond these resistless nanopatterning methods, another much simpler approach—stencil lithography—has also attracted intense attention in fabricating nanostructures [18–23]. Stencil lithography involves making of stencils which is a membrane that have patterns etched through and the stencil acts as a shadow mask through which evaporation of metals go through the stencils to form patterns on a substrate. Stencil lithography has unique advantages as compared to other patterning techniques: it does not require spinning of a uniform layer of resist (therefore patterns can be created on 3D topographies) and it does not involve any heat or chemical treatment of the substrate (like baking, developing and removing the resist). Thus, it allows a wide range of substrates (e.g., flexible, surface treated) and materials (e.g., organics) to be used. More importantly, stencils can be reused for multiple times by simply removing the metal residue with a mild metal etchant; moreover, stenciling has different working modes, i.e., static, multistep, and dynamic, hence allowing the structure fabrication with high-resolution, multi-mask and multi-material, arbitrary and three-dimensional, etc. Different areas of studies including (1) stencil making and increase its usability; (2) deposition condition through the holes; (3) making metallized free-standing membranes for direct use; and (4) deposition on various types of substrates which may be hard to achieve with traditional patterning techniques, such as silk, PDMS [20–23] have been carried out for stencil lithography technique.

E. S. P. Leong (✉) · J. Deng · Y. J. Liu · J. H. Teng (✉)
Institute of Materials Research and Engineering, Agency for Science, Technology and Research (A*STAR), 3 Research Link, Singapore 117602, Singapore
e-mail: leonge@imre.a-star.edu.sg

J. H. Teng
e-mail: jh-teng@imre.a-star.edu.sg

Fig. 1 Schematic of the fabrication process of the Si_3N_4 membrane stencil mask and the subsequent metamaterials structures using e-beam evaporator

1. Pattern on Si_3N_4 at back of Si **2. Etch Si_3N_4 to expose back of Si** **3. Etch Si by KOH** **4. Nanopatterning on Si_3N_4**

8. Deposit film on the membrane **7. Place the SiO_2 spacer layer in contact with quartz** **6. Deposit SiO_2 spacer layer** **5. Pattern transfer on Si_3N_4 via RIE**

Here, we apply direct patterning by stencil lithography to fabricate fishnet metamaterials nanostructures. We fabricate nanohole arrays on a Si_3N_4 membrane and then deposit multiple layers of metals and dielectrics and such approach allows us to have perforated fishnet metamaterial structures on the membrane as well as its complementary pillar structures on a quartz substrate. We then study and compare their optical properties from both experiment and simulation results.

2 Experiment details

2.1 Fabrication of Si_3N_4 membrane

The detailed fabrication process is illustrated in Fig. 1. First, we had a single side polished (100) Si wafer coated with 100 nm thick Si_3N_4 layer grown by low pressure chemical vapor deposition (LPCVD) technique. The Si wafer was about 250 μm thick and standard photolithography process was carried out on the backside of the wafer to open a 500 μm square window (step 1). The Si_3N_4 layer was etched with a reactive ion etcher (RIE), (Plasmalab 80plus, Oxford) using a mixture of fluoroform (55 sccm) and oxygen gas (5 sccm) at 55 mTorr chamber pressure and 175 W electric power for ∼3 min to expose the Si wafer (step 2). The wafer was then immersed in potassium hydroxide bath (30 wt%) at 60 °C to etch through the Si and leave behind a thin 100 nm thick Si_3N_4 membrane (step 3).

2.2 Nano-patterning on SiN membrane

A 170 nm thick ZEP-520A resist was spin-coated on to the membrane and soft-baked at 180 °C for 2 min. The designed patterns were written on the resist at a dose of 300 μC/cm^2 with an e-beam writer (ELS-7000, ELIONIX)

at an acceleration voltage of 100 kV and beam current of 50 pA. The exposed sample was then developed in Oxylene for 30 s and rinsed in IPA for 20 s (step 4). The resist patterns were transferred to the Si_3N_4 layer using RIE with the same recipe mentioned above. After that, the resist was removed in 1165 remover and rinsed with IPA and deionized water. The pattern size was ∼20 μm × 20 μm and periodic arrays of circular holes with diameter 110 ± 10 nm and pitch 200 nm were formed on the membrane (step 5).

2.3 Fabrication of metamaterial structures

A ∼300 to 500 nm thick silicon dioxide (SiO_2) spacer layer was deposited on to the membrane, with a 2 mm × 2 mm Si substrate covering the patterned region, using a plasma enhanced chemical vapor deposition (PECVD) system, (Nextral ND200, Unaxis) (step 6). The thickness of the spacer layer is selected such that it is about 50 nm thicker than the desired thickness of the deposited metal/dielectric layers. The patterned membrane with the SiO_2 spacer layer is then placed in contact with a quartz substrate and bonded with thermal tape (step 7). Finally, the samples are placed in an e-beam evaporator system (Denton Vacuum, Explorer) for alternate deposition of Au and MgF_2. The thickness of Au is ∼38 ± 3 nm, deposited at a deposition rate of 1.1 Å/s and the thickness of MgF_2 is ∼38 ± 8 nm at a deposition rate of 4Å/s. The base pressure is at 4e-7 Torr. Metal/dielectric/metal stacks of film are then formed on both the backside of the Si wafer and on the quartz substrate (step 8).

2.4 Spectral measurement

Unpolarized optical reflectance and transmission spectra were measured at normal incidence angle using a UV–VIS-

Fig. 2 **a** SEM image of the fishnet metamaterial structure on the Si$_3$N$_4$ membrane after depositing a stack of Au/MgF$_2$/Au. The observed reflected (**b**) and transmitted (**c**) optical microscopic images of the metamaterials structure. Measured (**d**) and simulated (**e**) reflection (*black curves*) and transmission (*blue curves*) spectra. Spectral fitting (*red curve*) to the transmission spectrum with the sum of two Lorentzian peaks (*green curves*) is demonstrated in **d**
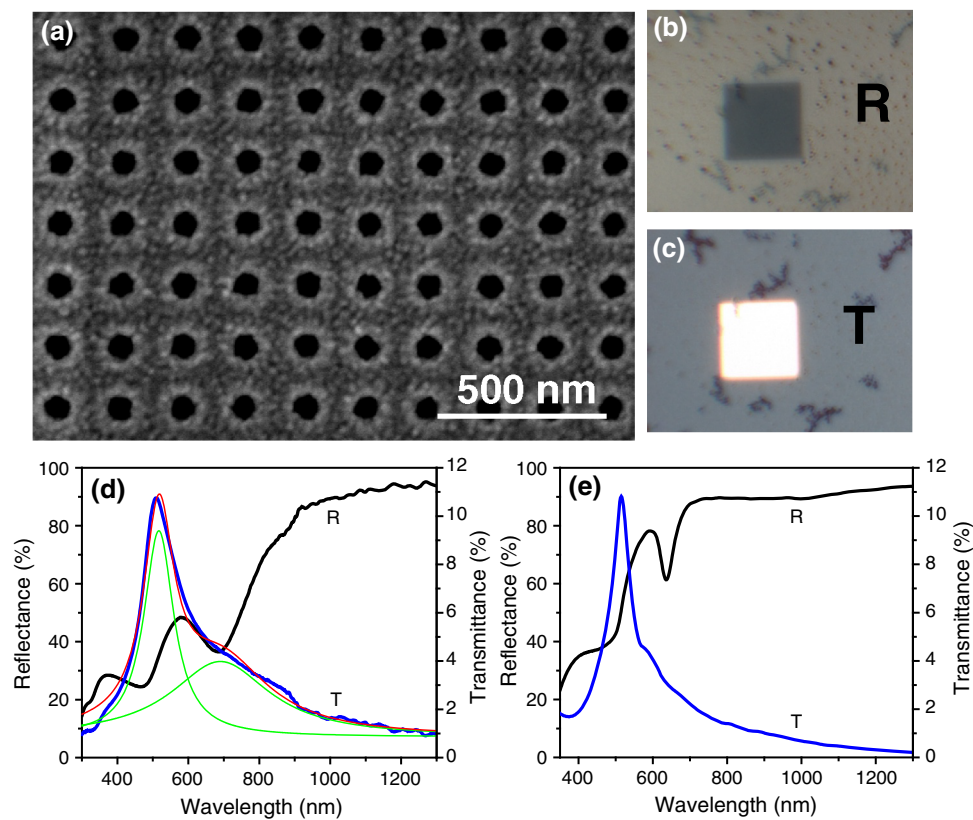
NIR microspectrophotometer (QDI 2010™, Craic). The probe light beam was focused to have a detecting area of 7.1 × 7.1 μm^2 using a 36 × objective lens combined with a variable aperture. Reflection and transmission measurements were normalized with respect to an aluminum mirror and a bare quartz substrate, respectively.

3 Results and discussion

Figure 2a shows a typical SEM image of a metamaterial structure after depositing a stack of Au/MgF$_2$/Au. We note that the nanohole size reduced slightly from ∼100 to ∼80 nm in diameter. Figure 2b–e shows the observed optical microscopic images and measured spectra in both reflection and transmission. From Fig. 2d, two regular dips in reflection at 686 and 465 nm can be clearly observed. Similar to the previous report [24, 25], the first dip is caused by the magnetic resonance around 686 nm, which comes from the coupling of the upper and lower layers in the magnetic strips. The second dip at 465 nm is formed by the electric resonance from the electric strips. As for the transmission spectrum, the spectral Lorentzian fitting clearly shows that the transmission spectrum is mainly contributed from two Lorentzian peaks, which correspond to the reflection dips. To confirm our results, we carried out

the FDTD simulations for this sample. In the simulation, we used the parameters and dimensions of the fabricated sample. The simulation results are shown in Fig. 2e. We can see that overall, the spectral features are in reasonable agreement between the simulation and experimental results even though there is a bit difference in terms of peak or dip positions. The observed difference could be mainly attributed to discrepancies between the material permittivities in the database of the software and real ones of the sample. As known, for the fishnet metamaterials, it is possible to achieve the negative refractive index in the range of the magnetic resonance [2, 24, 25]. Further details and retrieval of the refractive index will be discussed in a separate work.

Furthermore, we deposited three stacks of metal and dielectric layers and then characterized their optical properties. Figure 3a and b shows the SEM images of the original membrane nanohole structure before and after deposition of multiple stacks. When comparing Fig. 3a with b, we can see that the nanohole size reduces greatly from 120 to 60 nm in diameter. Therefore, we can foresee that the total number of layers that can be deposited is limited by the nanohole size. Figure 3c and d show the measured and simulated optical transmission and reflection spectra. Again, similar to the single stack case, two clear dips in reflection at ∼745 and ∼462 nm can be clearly

Fig. 3 SEM images of the original membrane nanohole structure before (**a**) and after (**b**) deposition of multiple stacks. Measured (**c**) and simulated (**d**) optical transmission and reflection spectra
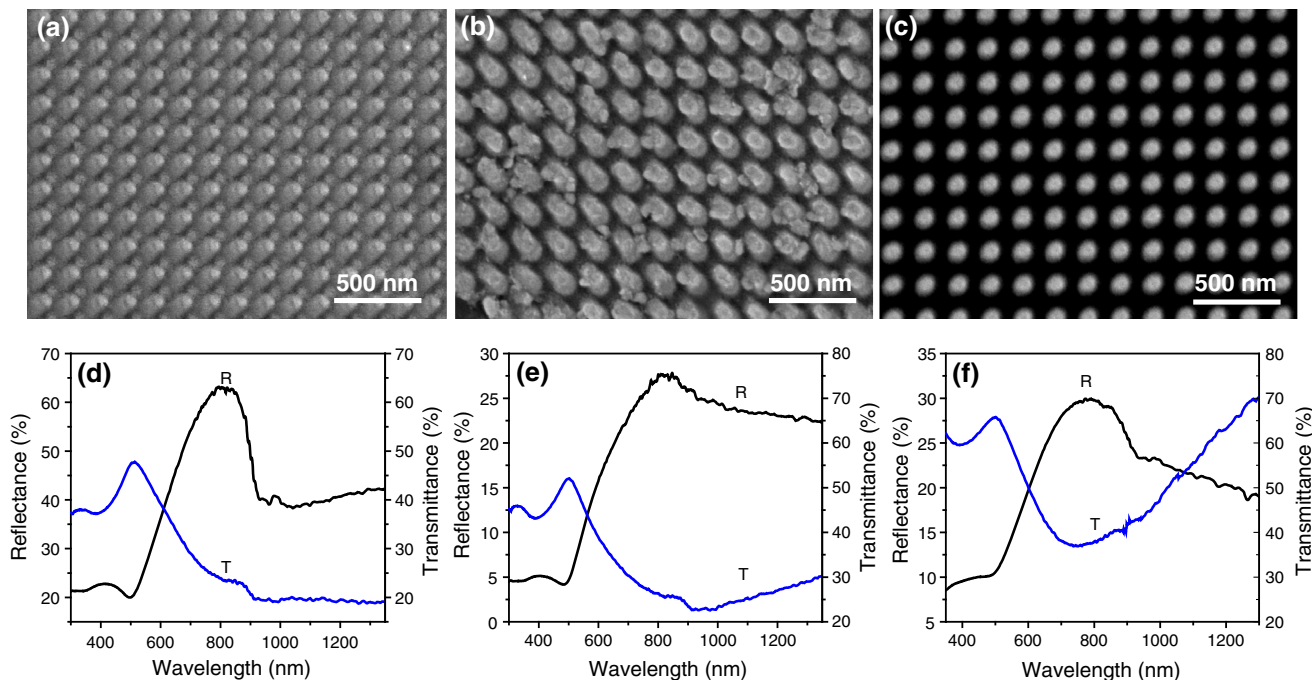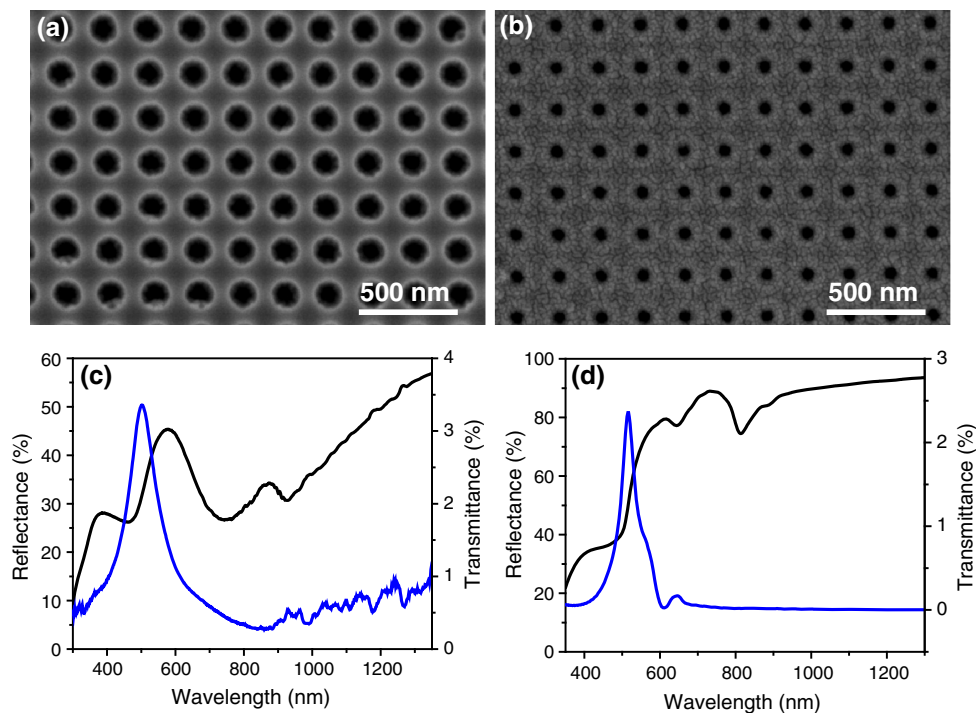
Fig. 4 SEM images of the fabricated pillar structures (**a**–**c**) and corresponding optical transmission and reflection spectra (**d**–**f**)

observed from the experimental results. In addition, another dip at ~927 nm appears in the measured reflection spectrum. When compared with the single stack case, the magnetic resonance of the fishnet metamaterials with multiple stacks has an obvious redshift, while the electric resonance keeps almost unchanged. The redshift of the magnetic resonance could be mainly attributed to the shrinkage of the nanoholes. The newly appeared reflection dip at ~927 nm arises from the hybridization of magnetic plasmons [25–27]. The simulated spectrum in Fig. 3d also shows the similar reflection dips, hence validating our experimental results.

For stencil lithography, in addition to achieve a perforated fishnet metamaterial structure on the membrane, we can also fabricate the membrane's complementary pillar structure on another substrate. Figure 4a–c show the SEM images of the fabricated pillar structures. We can see that the structure quality varies much, which is strongly dependent on the electron beam collimation during the deposition process. In general, a divergent electron beam makes the deposited material atoms highly diffused on to the quartz substrate beneath the membrane hole, hence leading to the formation of poor pillar structure in the interspacing. Moreover, a closer look shows that the formed pillars have a preferred tilt angle, as shown in both Fig. 4a and b. In contrast, a highly collimated electron beam makes the deposited material atoms deposited in a more defined way and hence a high-quality pillar structure is formed, as shown in Fig. 4c. The further spectral test also confirmed our analysis, as shown in Fig. 4d–f. As the multilayer pillars are more defined, an obvious transmission dip at ~750 nm appears and background transmitted light is also stronger.

4 Conclusion

In summary, we have demonstrated a high-resolution resistless nanopatterning technique based on the direct patterning by stencil lithography. Using this much simpler fabrication technique, fishnet metamaterial nanostructures and their complementary pillar nanostructures on a quartz substrate have been demonstrated. The experimental results showed that the stencil lithography allows much simpler nanopattern transfer to 100 nm thick Si_3N_4 as compared to etching of MDM stacked nanostructures. Fabrication of stacked perforated structure is much simplified as compared to traditional lift-off technique. The fabricated metamaterial structures have also shown the expected magnetic and electric resonances. The stencil lithography is a complementary alternative technique to fabricate nanoscale metamaterial structures.

References

1. N. Liu, H. Liu, S. Zhu, H. Giessen, Stereometamaterials. Nat. Photon. **3**, 157–162 (2009)
2. S. Xiao, V.P. Drachev, A.V. Kildishev, X. Ni, U.K. Chettiar, H.-K. Yuan, V.M. Shalaev, Loss-free and active optical negative-index metamaterials. Nature **466**, 735–738 (2010)
3. S. Larouche, Y.-J. Tsai, T. Tyler, N.M. Jokerst, D.R. Smith, Infrared metamaterial phase holograms. Nat. Mater. **11**, 450–454 (2012)
4. W. Cai, U.K. Chettiar, H.-K. Yuan, V.C. de Silva, A.V. Kildishev, V.P. Drachev, V.M. Shalaev, Metamagnetics with rainbow colors. Opt. Express **15**, 3333–3341 (2007)
5. E.S.P. Leong, Y.J. Liu, C.C. Chum, J.H. Teng, Optical magnetic resonances in subwavelength Ag-MgF2-Ag grating structures. Plasmonics **8**, 1221–1226 (2013)
6. T. Kraus, L. Malaquin, H. Schmid, W. Riess, N.D. Spencer, H. Wolf, Nanoparticle printing with single-particle resolution. Nat. Nanotech. **2**, 570–576 (2007)
7. Z.Y. Cai, Y.J. Liu, E.S.P. Leong, J.H. Teng, X.M. Lu, Highly ordered and gap controllable two-dimensional non-close-packed colloidal crystals and plasmonic-photonic crystals with enhanced optical transmission. J. Mater. Chem. **22**, 24668–24675 (2012)
8. Z.Y. Cai, Y.J. Liu, J.H. Teng, X.M. Lu, Fabrication of large domain crack-free colloidal crystal heterostructures with superposition bandgaps using hydrophobic polystyrene spheres. ACS Appl. Mater. Interfaces **4**, 5562–5569 (2012)
9. Z.Y. Cai, Y.J. Liu, X.M. Lu, J.H. Teng, In situ "doping" inverse silica opals with size-controllable gold nanoparticles for refractive index sensing. J. Phys. Chem. C **117**, 9440–9445 (2013)
10. D. Chanda, K. Shigeta, S. Gupta, T. Cain, A. Carlson, A. Mihi, A.J. Baca, G.R. Bogart, P. Braun, J.A. Rogers, Large-area flexible 3D optical negative index metamaterial formed by nanotransfer printing. Nat. Nanotech. **6**, 402–407 (2011)
11. S.Y. Yew, T.S. Kustandi, H.Y. Low, J.H. Teng, Y.J. Liu, E.S.P. Leong, Single-material-based multilayered nanostructures fabrication via reverse thermal nanoimprinting. Microelectron. Eng. **88**, 2946–2950 (2011)
12. Y.J. Liu, W.W. Loh, E.S.P. Leong, T.S. Kustandi, X.W. Sun, J.H. Teng, Nanoimprinted ultrafine line and space nanogratings for liquid crystal alignment. Nanotechnology **23**, 465302 (2012)
13. E.S.P. Leong, S.Y. Yew, T.S. Kustandi, Y.J. Liu, H. Tanoto, Q.Y. Wu, W.W. Loh, S.L. Teo, J.H. Teng, New approach for multilayered microstructures fabrication based on a water-soluble backing substrate. ACS Appl. Mater. Interfaces **5**, 5898–5902 (2013)
14. Y.J. Liu, G.Y. Si, E.S.P. Leong, N. Xiang, A.J. Danner, J.H. Teng, Light-driven plasmonic color filters by overlaying photoresponsive liquid crystals on gold annular aperture arrays. Adv. Mater. **24**, OP131–OP135 (2012)
15. Y.J. Liu, G.Y. Si, E.S.P. Leong, B. Wang, A.J. Danner, X.C. Yuan, J.H. Teng, Optically tunable plasmonic color filters. Appl. Phys. A **107**, 49–54 (2012)
16. G.Y. Si, Y.H. Zhao, J.T. Lv, M.Q. Lu, F.W. Wang, H.L. Liu, N. Xiang, T.J. Huang, A.J. Danner, J.H. Teng, Y.J. Liu, Reflective plasmonic color filters based on lithographically patterned silver nanorod arrays. Nanoscale **5**, 6243–6248 (2013)
17. G.Y. Si, Y.H. Zhao, J.T. Lv, F.W. Wang, H.L. Liu, J.H. Teng, Y.J. Liu, Direct and accurate patterning of plasmonic nanostructures with ultrasmall gaps. Nanoscale **5**, 4309–4313 (2013)
18. M.M. Deshmukh, D.C. Ralph, M. Thomas, J. Silcox, Nanofabrication using a stencil mask. Appl. Phys. Lett. **75**, 1631–1633 (1999)
19. A.A. Patel, C.P. Fucetola, E.E. Moon, H.I. Smith, 3D fabrication by stacking prepatterned, rigidly held membranes. J. Vac. Sci. Technol. B **29**, 06F402-1–06F402-3 (2011)
20. O. Vazquez-Mena, G. Villanueva, V. Savu, K. Sidler, M.A.F. van den Boogaart, J. Brugger, Metallic nanowires by full wafer stencil lithography. Nano Lett. **8**, 3675–3682 (2008)
21. O. Vazquez-Mena, T. Sannomiya, L.G. Villanueva, J. Voros, J. Brugger, Metallic nanodot arrays by stencil lithography for plasmonic biosensing applications. ACS Nano **5**, 844–853 (2011)

22. O. Vazquez-Mena, T. Sannomiya, M. Tosun, L.G. Villanueva, V. Savu, J. Voros, J. Brugger, High-resolution resistless nanopatterning on polymer and flexible substrates for plasmonic biosensing using stencil masks. ACS Nano **6**, 5474–5481 (2012)

23. H. Tao, J.J. Amsden, A.C. Strikwerda, K. Fan, D.L. Kaplan, X. Zhang, R.D. Averitt, F.G. Omenetto, Metamaterial silk composites at terahertz frequencies. Adv. Mater. **22**, 3527–3531 (2010)

24. S. Xiao, U.K. Chettiar, A.V. Kildishev, V.P. Drachev, V.M. Shalaev, Yellow-light negative-index metamaterials. Opt. Lett. **34**, 3478–3480 (2009)

25. N. Liu, L.W. Fu, S. Kaiser, H. Schweizer, H. Giessen, Plasmonic building blocks for magnetic molecules in three-dimensional optical metamaterials. Adv. Mater. **20**, 3859–3865 (2008)

26. T. Li, H. Liu, F.M. Wang, Z.G. Dong, S.N. Zhu, X. Zhang, Coupling effect of magnetic polariton in perforated metal/dielectric layered metamaterials and its influence on negative refraction transmission. Opt. Express **14**, 11155–11163 (2006)

27. H. Liu, D.A. Genov, D.M. Wu, Y.M. Liu, Z.W. Liu, C. Sun, S.N. Zhu, X. Zhang, Magnetic plasmon hybridization and optical activity at optical frequencies in metallic nanostructures. Phys. Rev. B **76**, 073101 (2007)